Available online at www.sciencedirect.com
ScienceDirect
Journal of Catalysis 242 (2006) 319–331
JOURNAL OF CATALYSIS
www.elsevier.com/locate/jcat

# Hydrogenation of Naphthalene over $NiO/SiO_2$–$Al_2O_3$ catalysts: Structure–activity correlation

Sharath R. Kirumakki [a], Boris G. Shpeizer [a], Guggilla Vidya Sagar [b], Komandur V.R. Chary [b], Abraham Clearfield [a,*]

[a] *Texas A & M University, Department of Chemistry, P.O. Box 30012, College Station, TX 77842-3012, USA*
[b] *Indian Institute of Chemical Technology, Catalysis Division, Hyderabad 500 007, India*

Received 22 March 2006; revised 3 June 2006; accepted 13 June 2006

Available online 26 July 2006

**Abstract**

A series of NiO–$SiO_2$–$Al_2O_3$ catalysts were synthesized by the sol–gel method. The samples were characterized by a wide array of techniques, including X-ray diffraction (XRD), transmission electron microscopy (TEM), X-ray photoelectron spectroscopy (XPS), $H_2$ temperature-programmed reduction (TPR), and temperature-programmed desorption (TPD) of $NH_3$. The nature of Ni species on the support and their interaction with the support was studied. XPS and TPR studies showed that Ni was present as $Ni^{2+}$ on the support, and that there was no $Ni^{3+}$ or $Ni^0$ in the unreduced samples. Two kinds of NiO were observed on the support, one in which the $Ni^{2+}$ interacts with the support and the other known as "free" NiO—that is, with no metal–support interactions. The reducibility of NiO decreased with increasing interaction with the support. The extent of interaction between the $Ni^{2+}$ and the support depended on the total Ni content of the sample and its Si/Al ratio. Increasing the Ni content in the material led to an increase in the relative concentration of free NiO, as well as an increase in the particle size of NiO as seen on TEM. An increase in Si content led to a decrease in the relative free NiO concentration and an increase in the total acidity of the sample, measured by $NH_3$-TPD. The impact of these effects on the catalytic activity of the samples was evaluated in the vapor-phase hydrogenation of naphthalene at 1 atm. A correlation was made between the catalytic activities and the relative concentration of free NiO. Hydrogenation of naphthalene proceeds sequentially by formation first of the partially hydrogenated tetralin and then of the fully hydrogenated decalin. The yield of decalin increased with increasing conversion of naphthalene; however, tetralin was the major product of this reaction. Kinetic studies were carried out to investigate the variation in selectivity with conversion of naphthalene. The reaction was best described using a two-site Langmuir–Hinshelwood model. The adsorption constants and of naphthalene, $K_N$, and tetralin, $K_T$, were $4.10 \times 10^{-3}$ and $1.88 \times 10^{-3}$ $m^3$/mol, respectively, at 200 °C. The low yield of decalin has been attributed to the weak adsorption of tetralin on the active site.
© 2006 Elsevier Inc. All rights reserved.

*Keywords:* Nickel–silica–alumina; Metal–support interactions; Reducibility; Hydrogenation; Naphthalene; Langmuir–Hinshelwood; Kinetics; Mechanism

## 1. Introduction

The design and characterization of new heterogeneous catalysts are of major interest for the development of new chemical processes of economic and ecologic interest to the chemical industry. Most industrial catalysts are high-surface area solids onto which an active component is dispersed in the form of very small particles (nanoparticles). The design of catalysts with controlled particle size and pores has been a fundamental objective of catalyst researchers [1]. The performance of a heterogeneous catalyst is a direct function of its chemical nature and/or its structure. High, homogeneous metal dispersion on the support is an important factor contributing to catalyst activity [2]. Metal–support interaction plays an important role in the catalytic activity of supported metal oxides [3]. The stronger the metal–support interaction, the higher the temperature of reduction of the metal. There are reports in the literature on the metal–support interactions over Ni catalyst with $SiO_2/Al_2O_3$ as support [4–8]. Strong Ni–support interactions hinder its activity in hydrogenation reactions but are found to favor reactions like $CH_4$ reforming with $CO_2$, for which it was found that cat-

* Corresponding author. Fax: +1 979 845 2370.
*E-mail address:* clearfield@mail.chem.tamu.edu (A. Clearfield).

0021-9517/$ – see front matter © 2006 Elsevier Inc. All rights reserved.
doi:10.1016/j.jcat.2006.06.014

alysts with a strong metal–support interaction were more active and showed greater resistance to coking and sintering than those that did not show a significant Ni–support interaction [4]. There is no general consensus on the extent and variation of the interaction of Ni atoms with the variation in Si/Al ratio of the support. Turlier et al. [5] studied the effect of different supports, including $Al_2O_3$ and $SiO_2$, on the reducibility of the metal deposited on these supports and concluded that the reducibility of Ni is greater over $Al_2O_3$ than over $SiO_2$. Amblard et al. [6] showed that for the Ni samples prepared by incipient wetness, the reducibility of $Ni^{2+}$ over $Al_2O_3$ is low compared with that over $SiO_2$. Jackson et al. [7] synthesized Ni catalysts by the impregnation method; in their system, the $Ni^{2+}$ in Ni–$SiO_2$ and Ni–$Al_2O_3$ reduced at identical temperatures, indicating a similar metal–support interaction in both the cases. Guimon et al. [8] studied the interactions of Ni with $SiO_2$–$Al_2O_3$ support prepared by the sol–gel technique and found that silica has very weak interactions with the metal. The addition of alumina to silica leads to the existence of two types of $Ni^{2+}$ crystallites, one presenting strong interactions with the support and the other presenting with very weak or no interactions. From the above discussion, it should be obvious that the Ni–support interaction is dependent on the synthetic route followed and varies from system to system. Therefore, it is imperative to understand the system thoroughly before testing it in any catalytic reaction.

The heterogeneous hydrogenation of naphthalene is not only a useful model reaction for gauging the activity of metal catalysts, but also is of commercial importance in the upgrading of coal liquids and diesel fuels [9]. The hydrogenated products are also proposed to act as hydrogen storage media for proton-exchange membrane fuel cells [10]. It is known that >60% of the C atoms in coal exist in aromatic forms, consisting mainly of 1–4 fused aromatic rings; thus, coal reactivity is strongly dependent on the aromatic structure. Because the large bonding energy of aromatic rings is lessened by reducing the C=C bonds to C–C bonds, the cracking reactivity of the polycyclic aromatic system can be greatly enhanced by hydrogenation of the aromatic rings [11]. The interest in low-aromatic-content diesel fuels has been stimulated in part by the discovery that diesel exhaust particles contain powerful carcinogens [12] and in part because the cetane number of low-quality diesel fractions can be increased by severely reducing their aromatic content [13]. If a deep aromatic saturation must be performed, then highly active hydrogenation catalysts working at moderate temperatures have to be prepared [14]. It is well established that noble metal catalysts have excellent hydrogenation properties at moderate pressures [8]. But these catalysts are expensive and are susceptible to deactivation by sulfur. There is a need to design highly active catalysts that can work under much milder reaction pressures and, if possible, use less expensive metals. Because of their low cost and acceptable resistance to sulfur poisoning, Ni-based systems are good alternatives to noble metal hydrogenation catalysts [15,16]. Hydrogenation of naphthalene has been carried out over supported Ni catalysts [17–21]. Barrio et al. [17] studied the vapor-phase hydrogenation of naphthalene over Ni and Ni–Pd supported on Si–Al mixed oxide systems and found that the specific activity does not depend on the details of the surface structure of the metal crystallites. Rautanen et al. [20] carried out hydrogenation in liquid phase over a commercial Ni–$Al_2O_3$ catalyst. They proposed that the hydrogenation of naphthalene to tetralin is structure-insensitive, whereas the hydrogenation of tetralin to decalin is sensitive to the catalyst structure. The hydrogenation activity of a catalyst varies depending on its synthesis and the reaction conditions.

We have synthesized a series of NiO–$SiO_2$–$Al_2O_3$ catalysts by the sol–gel method [22]. The main objective of this study was to characterize these materials to gain knowledge about the metal–support interactions. We have tried to understand the nature of the active species during the hydrogenation of naphthalene and to obtain a structure–activity correlation, if one exists. Kinetic studies described in this paper explain the variation in selectivity with conversion of naphthalene.

## 2. Experimental

### 2.1. Catalyst preparation

The catalysts used in this study, NiO–$Al_2O_3$–$SiO_2$, were prepared by a sol–gel method using aluminum-*tri-sec*-butoxide (Aldrich) as the Al precursor, tetraethylorthosilicate (Aldrich) as the Si source, and $Ni(CH_3COO)_2{\cdot}4H_2O$ (Aldrich) as the Ni source [22]. In a typical procedure, to 50 mmol of tetraethylorthosilicate (TEOS) in a beaker is added 67.5 mmol of aluminum-*tri-sec*-butoxide. After stirring, 25 mmol of Ni acetate is then added, followed by the dropwise addition of 16 mmol of propylamine. *n*-Propanol (16 mmol) and $H_2O$ (50 mmol) are added dropwise while stirring. After stirring for 3 h, the mix is evaporated to dryness at 130 °C in an oven and heated to 400 °C in a static furnace to remove the organic matter. The amount of Al, Si and Ni precursors was varied to obtain catalysts with differing Si/Al ratios and Ni concentrations.

### 2.2. Catalyst characterization

#### 2.2.1. Elemental analysis

Ni content was estimated using atomic absorption spectroscopy (AAS) after dissolving the sample in HF on a Varian 250 AA system.

#### 2.2.2. X-ray diffraction

X-ray diffraction (XRD) patterns were obtained with a Bruker D 8 diffractometer, using Cu$K\alpha$ radiation (1.5406 Å) at 40 kV and 40 mA and a diffracted beam graphite monochromator. The measurements were recorded in steps of 0.04° with a count time of 1 s in the $2\theta$ range of 2°–60°.

#### 2.2.3. Surface area, pore size measurements

The BET surface area of the samples was determined from multipoint BET isotherms (Quantachrome Autosorb-1) using nitrogen as adsorbate at 77 K. Before the measurement, the samples were degassed at 225 °C for 12 h.

#### 2.2.4. Temperature-programmed reduction and desorption studies

Temperature-programmed reduction (TPR) of $H_2$ and temperature-programmed desorption (TPD) of $NH_3$ were carried out on Auto Chem 2910 (Micromeritics) instrument to study the reducibility of NiO supported on $SiO_2$–$Al_2O_3$ and the acidity of the system. In a typical experiment, 250 mg of oven-dried sample (dried at 100 °C for 15 h) was taken in a U-shaped quartz sample tube. The catalyst was mounted on a quartz wool plug. Before the studies, the sample was pretreated by passing argon over the catalysts at a flow of 50 ml/min at 100 °C for 2 h. After pretreatment, the sample was cooled to ambient temperature and TPR analysis was carried out in a flow of 10% $H_2$–Ar (50 ml/min) from ambient temperature to 700 °C at a heating rate of 10 °C/min.

For the TPD studies, after pretreatment, the sample was reduced at 300 °C for 2 h by passing pure hydrogen (99.99%, 75 ml/min) and was subsequently flushed with pure helium (50 ml/min) for 30 min to remove excess hydrogen. After the sample was reduced, it was saturated with $NH_3$ in a flow of 10% $NH_3$–He mixture (75 ml/min) for 1 h at 80 °C, then flushed with pure helium (50 ml/min) at 100 °C for 1 h to remove physisorbed $NH_3$. TPD analysis was carried out from ambient temperature to 500 °C at a heating rate of 10 °C/min in a He flow of 50 ml/min. H2 consumption, $NH_3$ desorption, and $T_{max}$ positions were calculated using GRAMS/32 software.

#### 2.2.5. X-ray photoelectron spectroscopy

X-ray photoelectron spectroscopy (XPS) was done with a Kratos Axis Ultra Imaging X-ray photoelectron spectrometer equipped with a Mg anode and a multichannel detector. Charge referencing was measured against adventitious carbon (C 1s, 284.8 eV). Shirley-type background was subtracted from the signals. The recorded spectra were always fitted using Gauss–Lorentz curves to determine the binding energy of the different element core levels more accurately.

#### 2.2.6. Transmission electron microscopy

Transmission electron microscopy (TEM) was performed with a JEOL JEM 2010 high-resolution transmission electron microscope. The samples were dispersed in methanol solution and suspended on a 400-mesh, 3.5-mm-diameter Cu grid.

### 2.3. Catalytic activity

The reaction was performed in a fixed-bed continuous-flow quartz catalytic reactor (10 mm i.d.) operated in the down-flow mode at atmospheric pressure. The reaction temperature was measured with a thermocouple in contact with the catalyst bed. The organic feed consisted of a solution of naphthalene in toluene (2.5–20 wt%) and was fed into the reactor by a piston pump. A fixed volume of catalyst (3 $cm^3$ with a particle size of 0.85–1.00 mm) diluted with SiC was used in all cases. Before the activity tests, the catalysts were reduced in situ at atmospheric pressure with $H_2$ (flow rate 20 $cm^3$/min) at 200–450 °C for 7 h, with a heating rate of 3 °C/min. The liquid products were collected at the bottom of the reactor for 1 h using a trap cooled in ice. The products were analyzed using an Agilent 6890 N gas chromatograph (flame ionization detector, HP-5 column, 30 m × 5 mm × 0.25 μm) and confirmed by gas chromatography–mass spectroscopy (GC-MS). The only products detected were tetralin and decalin; there were no products due to ring opening and hydrogenolysis. Toluene was not hydrogenated during the reaction. Blank reactions were carried out in the absence of a catalyst but with the same amount of SiC as in the catalytic reaction, and no products were detected. The conversion and selectivity were calculated based on the GC results. The rate of the reaction was calculated based on the equation

$$r_{\mathrm{Naph}} = \frac{F X_{\mathrm{Naph}}}{W},$$

where $r_{\mathrm{Naph}}$ is the rate of hydrogenation of naphthalene (mmol/(h g)), $F$ is the flow rate of naphthalene (mmol/h), $X_{\mathrm{Naph}}$ is the fractional conversion of naphthalene, and $W$ is the weight of the catalyst (g).

## 3. Results and discussion

### 3.1. Catalyst characterization

The catalysts were characterized to elucidate the nature of Ni species present on the surface and the role of these species in the catalytic reaction. In addition to metal centers, the acid sites of support also play a role in aromatic hydrogenation [23]. The acidity of the samples can be altered by varying the Si/Al ratio. The effects of varying Si/Al ratio on crystallinity, metal oxide distribution, metal–support interaction, and acidity were also studied. For this purpose, two series of catalysts were prepared, one with a Ni loading of 5–67 wt% and a constant Si/Al ratio of around 11 and the other with a Ni content of 11 wt% and a varying Si/Al ratio.

#### 3.1.1. BET surface area

The BET surface areas determined by nitrogen physisorption of all the catalysts are presented in Table 1. The BET surface area as well as the pore volume decreased as a function of Ni loading on $Al_2O_3$–$SiO_2$. This may be due to the formation of

Table 1
BET surface area and pore size of NiO–$SiO_2$–$Al_2O_3$ samples calcined at 500 °C

| Ni (wt%) | Si/Al | Surface area ($m^2$/g) | Total pore volume ($cm^3$/g) |
|---|---|---|---|
| 6.8 | 11.3 | 572 | 0.263 |
| 11.4 | 11.3 | 548 | 0.247 |
| 11 | Si | 559 | 0.35 |
| 11 | 0.46 | 453 | 0.227 |
| 11 | Al | 354 | 0.204 |
| 15 | 11.3 | 480 | 0.224 |
| 19 | 11.4 | 387 | 0.258 |
| 40 | 11.2 | 270 | 0.095 |
| 67 | 11 | 171 | 0.134 |

large NiO particles on the pore walls. The surface area also varied with the Si/Al ratio. The NiO sample containing only silica as the support had the highest surface area (559 $m^2/g$); surface area decreased with increasing $Al_2O_3$ content in the matrix.

### 3.1.2. XRD

The XRD patterns of the samples with different Ni loadings are presented in Fig. 1. No peaks due to $Al_2O_3$ or $SiO_2$ can be seen, implying that $Al_2O_3$–$SiO_2$ exists as an amorphous or poorly crystalline phase. It can be seen that the samples were amorphous at low Ni loading. Peaks at $2\theta = 37.13°$ and 43.24° ($d = 2.42$ and 2.09) were visible at Ni loading of around 21 wt%. These characteristic diffraction lines of cubic NiO crystals became prominent only when the Ni loading was around 40 wt%, demonstrating that the NiO particles were small and well dispersed at loadings <40 wt%. Samples with pure $SiO_2$ as support and pure $Al_2O_3$ as support showed no crystallinity, indicating that $SiO_2$ and $Al_2O_3$ existed as amorphous phases. Peaks due to NiO were seen only in the sample with pure $Al_2O_3$ as the support. The NiO peaks were very weak and broad in this case, indicating small particle size.

### 3.1.3. TEM

Representative transmission electron micrographs of the samples and the particle size distribution are shown in Figs. 2 and 3, respectively. All of the micrographs exhibit a uniform dispersion of NiO particles with a narrow particle size range on the support. The NiO particle size increased with increasing Ni loading. Most of the NiO particles were in the 7.6-nm range at a Ni loading of 11 wt%. The maximum shifted to the 17.6–20 nm region when the Ni loading was increased to 40 wt%. At very high Ni loadings (67 wt%), NiO crystallites in the 25-nm range

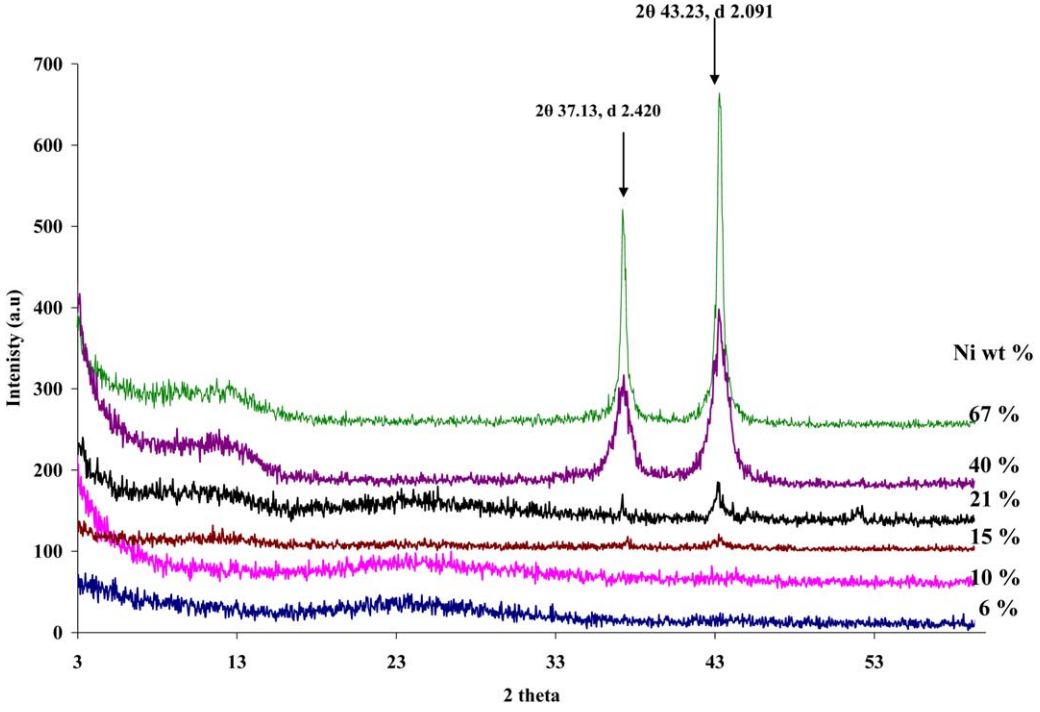


Fig. 1. X-ray diffraction pattern of calcined NiO–$SiO_2$–$Al_2O_3$ samples with different Ni loadings, Si/Al ∼ 11.

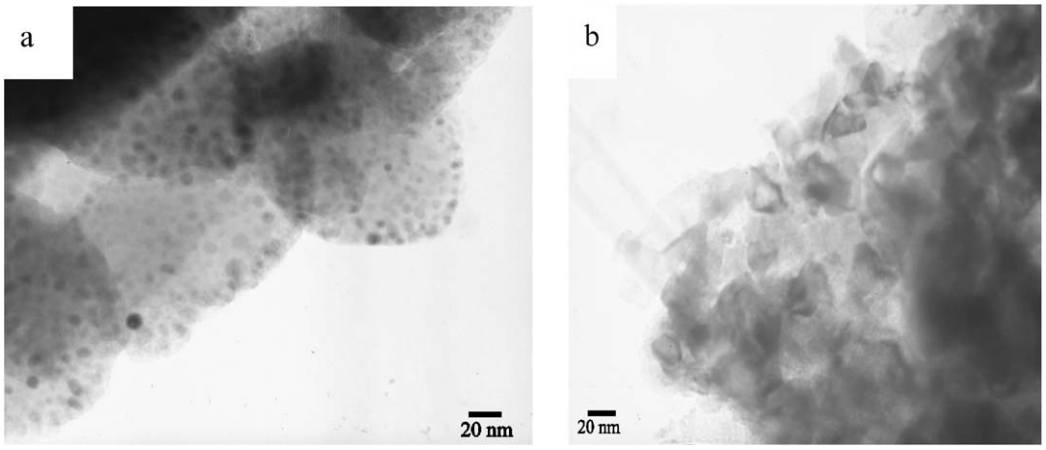


Fig. 2. TEM micrographs of calcined NiO–$Al_2O_3$–$SiO_2$ samples: (a) 11 wt% Ni and (b) 67 wt% Ni.

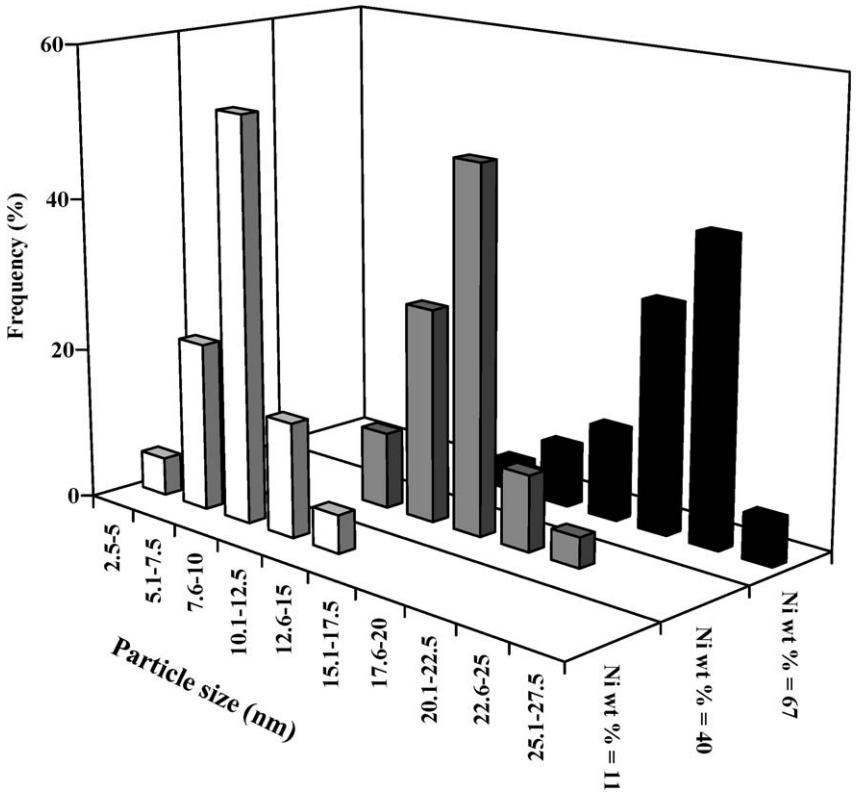


Fig. 3. Size distribution histogram of NiO particles in the calcined NiO–$SiO_2$–$Al_2O_3$ system.

were formed on the $SiO_2$–$Al_2O_3$ support. The NiO particle size did not vary much with the Si/Al ratio, remaining within the 7.5–10 nm range over both pure $SiO_2$ and pure $Al_2O_3$ supports.

### 3.1.4. XPS

The binding energies of electrons determined by XPS provide useful information on the oxidation states of different elements. A typical Ni $2p_{3/2}$ XPS spectrum of the sample shows peaks at 855.4 eV, 856.8 eV, and a broad peak at around 861 eV (Fig. 4). The component at 854.5 eV (with satellites at 861.7) is attributed to $Ni^{2+}_{oc}$ of NiO ($Ni^{2+}$ in an octahedral geometry) [24]. It is noteworthy that the reducibility of $Ni^{2+}_{oc}$ was greater than that of $Ni^{2+}_{T}$ ($Ni^{2+}$ in a tetrahedral geometry). The shift between the satellite and the main peak was about $6 \pm 1$ eV; the shift and the relative intensities depend generally on the nature of the environment and on the electronic charge of the metal (i.e., the oxidation state and the interaction with support). It is difficult to analyze these shifts and intensities for these samples because of the presence of more than one type of $Ni^{2+}$ species on the surface. The peak at 856.8 eV can be attributed to $Ni^{2+}$ of NiO interacting with the support or Ni silicate/aluminate or $Ni^{3+}$. XPS of samples with increasing Ni loading shows a clear increase in the intensity of the NiO peak (Fig. 4). Ni $2p_{3/2}$ XPS of the samples with differing Si/Al ratios, except the one with pure $Al_2O_3$ as support, showed only two peaks, at 856.8 and 861 eV, which are characteristic of $Ni^{2+}$ in the NiO species interacting with the support. The $Al_2O_3$ sample had an additional peak at 854.5 eV, corresponding to the free NiO. This indicates that interaction between $Ni^{2+}$ and $Al_2O_3$ is lower than the interaction between $Ni^{2+}$ and $SiO_2$. A plot of relative concentration of NiO (from XPS) as a function of total Ni content (from elemental analysis) shows a linear increase (Fig. 5). This suggests that as the Ni loading increased, the relative concentration of NiO with no interaction with the support also increased.

### 3.1.5. TPR

XPS and TPR are complimentary techniques that when used in conjunction help identify the oxidation states of a reducible metal oxide and estimate the interaction of the metal oxide with the support. The TPR profiles of the samples are presented in Fig. 6. The presence of $Ni^{3+}$ in the sample can be precluded by the absence of a reduction peak at 200 °C [25]. The peak with $T_{max}$ at 300 °C can be attributed to the reduction of NiO particles with no interaction with the support [26,27]. The interaction of NiO with the support decreases its reducibility [3,28]. The peak with $T_{max}$ at around 450 °C thus can be assigned to the $Ni^{2+}$ of the NiO species interacting with the support, and not due to the Ni silicate/aluminate peak, because the reduction peak of Ni silicate/aluminate would appear at a much higher temperature. The peak at $T_{max} = 580$ °C observed at a Ni loading of 67% may be due to the formation of amorphous Ni silicate/aluminate species. Quantification of the TPR curves (Fig. 7) shows that hydrogen consumption was linearly dependent on the wt% of Ni in the catalysts, and hydrogen consumption corresponded to the total reduction of all of the different Ni ions from +2 to the metallic form. $Ni^{2+}$ was reduced to $Ni^0$ in a single step. The TPR study clearly demonstrates the differences in the interactions between $Ni^{2+}$ and the support with varying

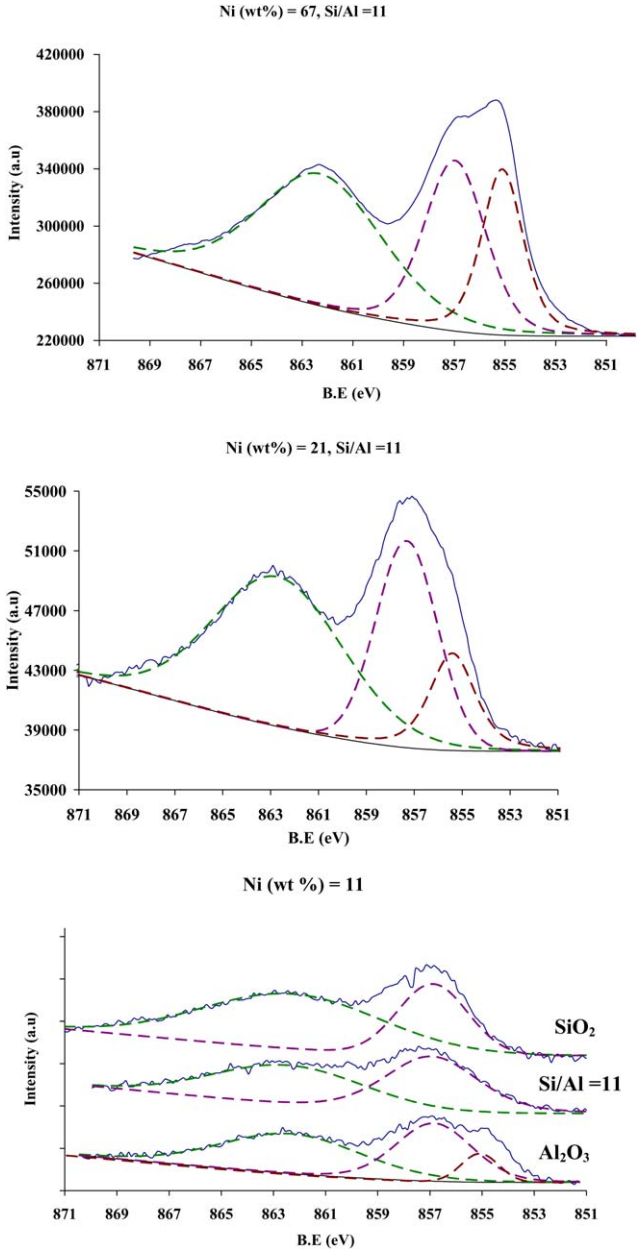


Fig. 4. XP Ni $2p_{3/2}$ spectra of calcined NiO–$SiO_2$–$Al_2O_3$ samples.

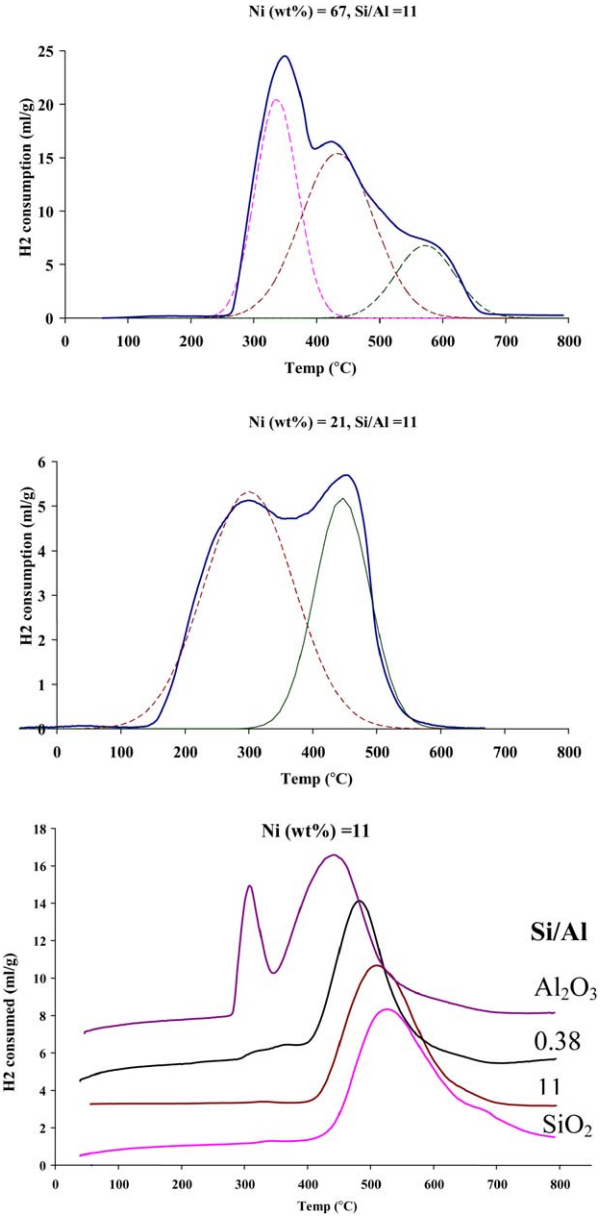


Fig. 6. TPR profiles of calcined NiO–$SiO_2$–$Al_2O_3$ samples.

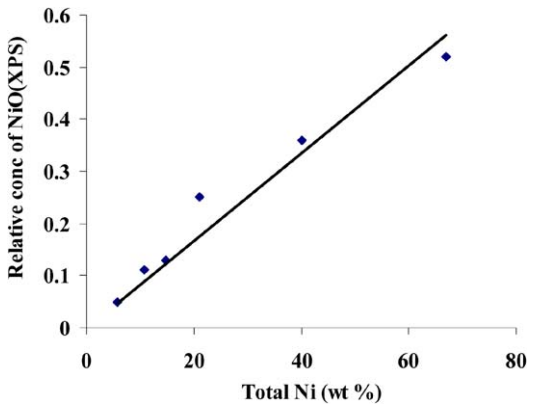


Fig. 5. Plot of relative concentration of NiO determined by XPS as a function of total Ni content determined by elemental analysis.

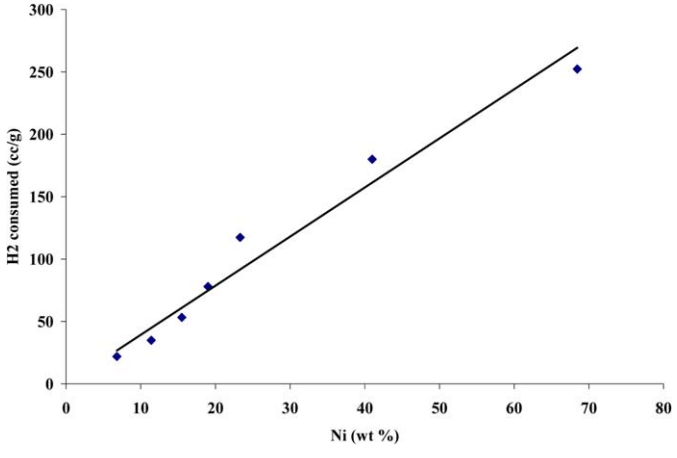


Fig. 7. A plot of amount of $H_2$ consumed during the TPR of NiO–$SiO_2$–$Al_2O_3$ samples as a function of total Ni content (Si/Al ∼ 11).

Table 2
$NH_3$ desorbed during the TPD experiments over $NiO–SiO_2–Al_2O_3$ samples with ~11 wt% Ni and different Si/Al ratios

| Si/Al | Weak[a] ml/g $NH_3$ ($T_{max}$ (°C)) | Moderate[a] ml/g $NH_3$ ($T_{max}$ (°C)) | Strong[a] ml/g $NH_3$ ($T_{max}$ (°C)) | Total $NH_3$ (ml/g) |
|---|---|---|---|---|
| $Al_2O_3$ | 19.7 (222) | 22.2 (319.1) | 14.08 (384) | 55.98 |
| 0.22 | 17.44 (220.9) | – | 44.20 (395) | 61.64 |
| 0.48 | 18.68 (224.5) | – | 45.98 (405) | 64.66 |
| 2.27 | 14.48 (218.5) | – | 46.86 (412) | 61.34 |
| $SiO_2$ | 16.69 (223.4) | – | 50.35 (436) | 67.04 |

[a] Weak = 150–250 °C, moderate = 250–350 °C, and strong = 350–450 °C.

Si/Al ratio. The TPR profile shows that the reducibility of the $Ni^{2+}$ species increased with increasing Al content. The interaction between $Ni^{2+}$ and the support increased with increasing Si content. This leads to a shift in the $T_{max}$ value of peaks corresponding to the reduction of $Ni^{2+}$ species interacting with the support from around 425 °C over $Al_2O_3$ to around 550 °C over $SiO_2$. A peak due to the reduction of free NiO was seen only in samples with high Al content. In samples with high Si content, a small peak above 600 °C was seen, most probably due to the formation of amorphous or poorly crystalline Ni silicate species, which were not visible in the XRD patterns (Fig. 1).

From the TPR and XPS study, it can be concluded that the Ni was present as NiO on the catalyst, and no $Ni^{3+}$ was present in the sample. Two kinds of NiO were observed on the support, one in which the $Ni^{2+}$ interacts with the support and the other as "free" NiO—that is, with no metal–support interactions. The relative concentration of free NiO increased; that is, the metal–support interaction decreased with increasing metal loading as well as increased $Al_2O_3$ content in the catalyst.

### 3.1.6. TPD

The acidity of the sample was estimated by TPD of $NH_3$. The strength of the acid sites can be determined by the temperature at which the adsorbed $NH_3$ desorbs. Based on the desorption temperature, the acid sites can be classified as weak (150–250 °C), medium (250–350 °C), or strong (350–450 °C) [28]. The data were treated mathematically, and the peaks were fitted using a Gaussian function. All of the samples had a peak in the weak acid site region (i.e., $T_{max}$ 150–250 °C) and another in the strong acid site region ($T_{max}$ 350–450 °C). The catalyst with pure $Al_2O_3$ as the support had an additional peak in the medium acid site region ($T_{max}$ = 318 °C). The $T_{max}$ of the peak corresponding to the strong acid site decreased with increasing Al content in the support, whereas the $T_{max}$ value of the weak acid site remained constant at around 220 °C. The total acidity of the sample decreased with decreasing $SiO_2$ content (Table 2). A similar trend has been reported in the literature [29].

## 3.2. Catalytic activity

Preliminary investigations were carried out on the effect of various reaction parameters on the hydrogenation of naphthalene to optimize the reaction conditions.

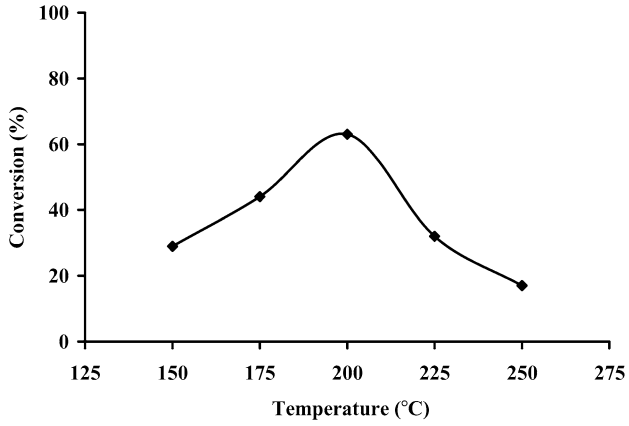


Fig. 8. Hydrogenation of naphthalene over $NiO–SiO_2–Al_2O_3$: effect of reaction temperature; WHSV = 0.4 $h^{-1}$ w.r.t. naphthalene, reduction temperature = 250 °C, $H_2$ = 19 ml/min. Catalyst: Ni = 15%, Si/Al = 11.

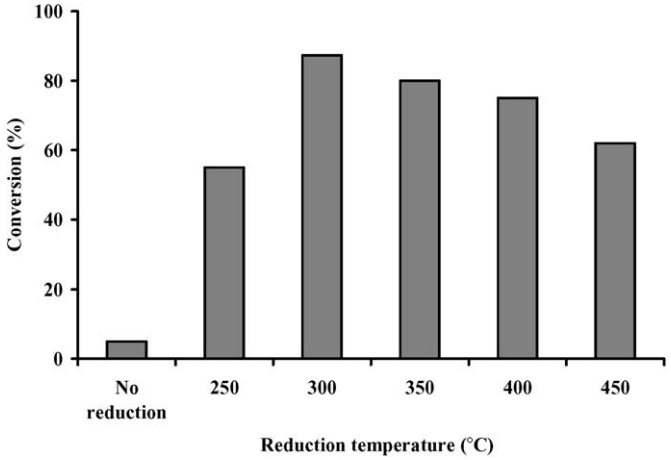


Fig. 9. Hydrogenation of naphthalene over $NiO–SiO_2–Al_2O_3$: effect of reduction temperature; WHSV = 0.4 $h^{-1}$ w.r.t. naphthalene, $H_2$ = 19 ml/min. Catalyst: Ni = 15%, Si/Al = 11.

### 3.2.1. Effect of reaction temperature

Reactions were carried out at 150–250 °C. The conversion of naphthalene increased from 29 to 63% on increasing the reaction temperature from 150 to 200 °C (Fig. 8) but decreased at temperatures above 200 °C. Hydrogenation is an exothermic reaction that does not favor high reaction temperatures. This Ni catalyst proved to be highly reactive at 200 °C. No high-molecular-weight products were observed at higher reaction temperatures.

### 3.2.2. Effect of reduction temperature

The catalysts were reduced for 7 h in $H_2$ flow at temperatures ranging from 250 to 450 °C. The effect of reduction temperature on the conversion of naphthalene is shown in Fig. 9. The conversion of naphthalene increased from 55 to 87% on increasing the reduction temperature from 250 to 300 °C. A further increase in the reduction temperature led to decreased conversion. Sintering of the Ni occurs at temperatures above 300 °C [18,30]. The unreduced Ni sample gave a 5% conversion of naphthalene to tetralin.

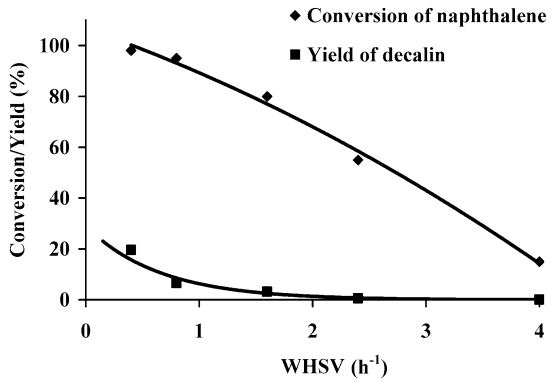


Fig. 10. Hydrogenation of naphthalene over NiO–$SiO_2$–$Al_2O_3$: effect of WHSV; reduction temperature = 300 °C, reaction temperature = 200 °C, $H_2$ = 19 ml/min. Catalyst: Ni = 15%, Si/Al = 11.

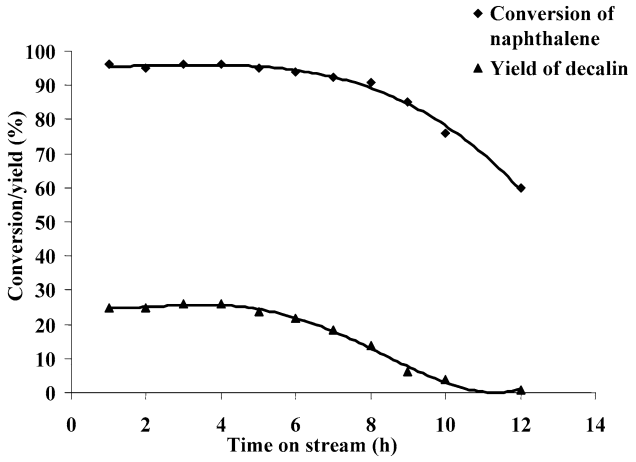


Fig. 11. Hydrogenation of naphthalene over NiO–$SiO_2$–$Al_2O_3$: time on stream study; WHSV = 0.4 $h^{-1}$ w.r.t. naphthalene, reaction temperature = 200 °C, reduction temperature = 300 °C, $H_2$ = 19 ml/min. Catalyst: Ni = 67%, Si/Al = 11.

### 3.2.3. Effect of WHSV

The hydrogenation of naphthalene was carried out at 200 °C with WHSV varying from 0.4 to 4 $h^{-1}$. It was seen that as the WHSV increased, the conversion of naphthalene decreased (Fig. 10). The formation of decalin occurred only at high naphthalene conversion, and as WHSV increased, the yield of decalin fell exponentially. The conversion decreased from 98% at 0.4 $h^{-1}$ to 80% at 1.5 $h^{-1}$, and the yield of decalin fell from 20 to 3% during this period. A further decrease in conversion on increasing WHSV led to a drop in the decalin yield to <0.5%.

From the above preliminary studies, the following reaction parameters were chosen: reduction temperature, 300 °C; reaction temperature, 200 °C; WHSV, 1 $h^{-1}$. Time on stream studies showed that the conversion of naphthalene was stable up to around 8 h of reaction, after which considerable loss of catalytic activity occurred (Fig. 11). The yield of decalin was also stable up to 8 h, and there was a decrease in decalin formation from around 14–0.5% with a decrease in conversion from 90 to 60%.

## 3.3. Studies on the reduced catalyst

The effect of reduction on the catalyst was studied by XPS, TPR, and TEM techniques. The TEM image of the reduced and the unreduced catalyst is shown in Fig. 12. It appears that agglomeration of Ni particles occurs on reduction. Most of the NiO particles were in the 5–10 nm range before reduction; on reduction, the particle size distribution broadened, with 50% of the particles being in the 30–40 nm range. XPS analyses of this catalyst before and after reduction showed that only about 35% of the total Ni was reduced (Fig. 13). All of the free NiO species were reduced, as demonstrated by the absence of a peak at 854 eV; the peak at 852 eV corresponds to $Ni^0$ [23]. Only 20% of the NiO species interacting with the support were reduced. This was further confirmed by the TPR studies (Table 3). The reduced samples showed no $H_2$ uptake at 300 °C, implying that all of the free NiO species were reduced to Ni. $H_2$ consumption of the samples at 400 °C decreased by around 20% after reduction, again suggesting that only a fraction of the NiO particles interacting with the support were reduced. The hydrogenation reaction was catalyzed by $Ni^0$; the unreduced $Ni^{2+}$ did not play a significant role in catalyzing the reaction.

### 3.3.1. Effect of NiO content

It was observed that the conversion of naphthalene increased with increasing Ni content (Table 4). The conversion of naphthalene was 20% when the Ni content was 6.8% and increased to 88% when the Ni content was increased to 67%. The XPS and TPR results clearly show that the relative concentration of free NiO increased with Ni loading, and because the hydrogenation of naphthalene is dependent on the $Ni^0$, the conversion of naphthalene increased with increasing Ni loading. Under the present reaction conditions, conversion of naphthalene was directly proportional to the amount of free NiO present, because this was the most easily reducible species. Transformation of naphthalene to decalin was observed only at very high naphthalene conversion; for example, the decalin yield was 0.2% at a naphthalene conversion of 40% and 12% at a naphthalene conversion of 88%. This implies that decalin was formed only at high tetralin concentration. This dependence has been observed by other researchers during the hydrogenation of naphthalene [31,32]. We discuss the reason for this later in the article. Although the surface area of the samples decreased with Ni loading, this did not seem to have any significant effect on naphthalene conversion. The hydrogenation of aromatic compounds has been reported to be dependent on the size of the supported metal oxide particle [33]. Hydrogenation of phenol over Ni and Pd catalysts was found to be largely structure-insensitive, although a sharp decline in the rate was observed at particle sizes <2 nm [34,35]. In the present study it was not possible to distinguish between the effect of particle size and relative concentration of free NiO, because both of these parameters increased with increasing Ni content. The easier reducibility of free NiO and a direct correlation between the free NiO and conversion of naphthalene indicates that this is a more dominant effect.

### 3.3.2. Effect of Si/Al ratio

To study the effect of Si/Al ratio on the activity, the WHSV of the reactant was increased from 0.4 to 3.3 $h^{-1}$ (with respect to naphthalene) to obtain a lower conversion that would make the comparison of the catalytic activity more meaning-

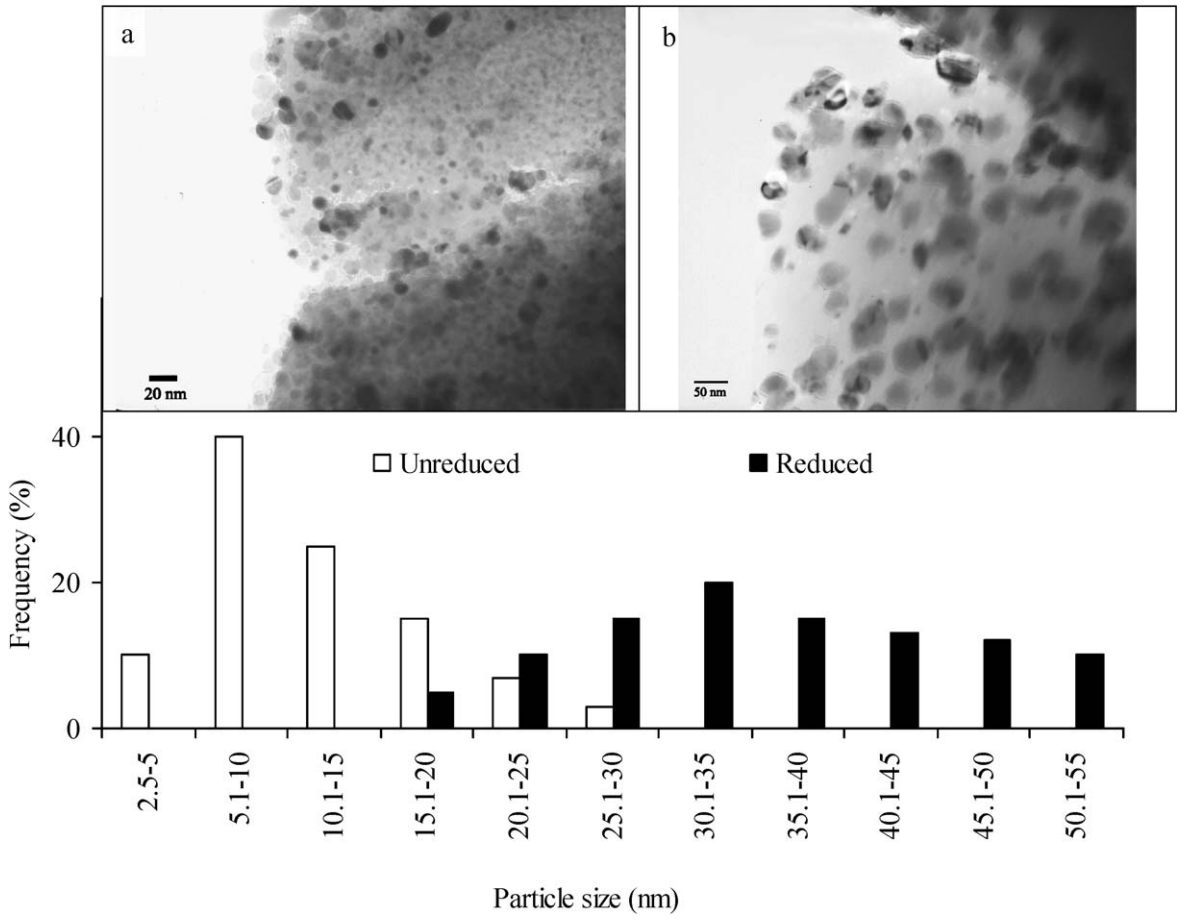


Fig. 12. TEM and histogram of the (a) unreduced and (b) reduced samples of $NiO–SiO_2–Al_2O_3$; 15 wt% Ni, Si/Al = 11.

Table 3
Comparison of $H_2$ consumption during TPR of unreduced samples and samples reduced at 300 °C for 7 h

| Ni (wt%) | TPR of unreduced sample, $H_2$ consumption (ml/g) | | | TPR of sample reduced at 300 °C, $H_2$ consumption (ml/g) | |
|---|---|---|---|---|---|
| | $T_{max}$ 300 °C | $T_{max}$ 400 °C | $T_{max}$ 580 °C | $T_{max}$ 400 °C | $T_{max}$ 580 °C |
| 15 | 12.05 | 38 | – | 30.5 | – |
| 67 | 101 | 102.3 | 44.5 | 78 | 43 |

ful. However, the samples had vastly different catalytic activity, and hence the conversions were not low in all cases, as shown in Fig. 14. Of all of the different catalysts tested, NiO on $Al_2O_3$ gave the best result, with a naphthalene conversion of 90%. As the Al content in the sample decreased, the conversion of naphthalene decreased; on the pure $SiO_2$ support, a naphthalene conversion of 8% was observed. There are two possible reasons for this: (1) decreased acidity of the sample and (2) increased reducibility of NiO with increasing Al content.

Venezia et al. [23] reported a correlation between the concentration of the medium-strength acid sites and the turnover frequencies in hydrogenation of naphthalene. However, in our samples the change in acidity was not as significant as the variation in reducibility of Ni species with varying Si/Al ratios. Therefore, the more likely reason was that as the Al concentration increased, the free NiO concentration increased. Thus, after reduction of the catalyst at 300 °C, the number of reduced Ni species would be greater in samples with higher Al content. As mentioned earlier, $Ni^0$ is the active species in the hydrogenation reaction. Therefore, samples with high $Al_2O_3$ content would be more active than samples with high $SiO_2$ content. Our results agree with this prediction.

## 4. Mechanism of hydrogenation

Hydrogenation of naphthalene was carried out at atmospheric pressure with a hydrogen/naphthalene mole ratio of 100. The conversion of naphthalene was maintained at <15% by increasing the WHSV to 8 $h^{-1}$. Hydrogenation of naphthalene proceeds through a sequential pathway forming tetralin first by hydrogenation of one ring and *cis* and *trans* decalin by hydrogenation of the second ring. Although there is almost no contradiction to the fact that decalin is formed only at very high naphthalene conversion, the reason for this is still not clear. Corma et al. [36] reported that the rate of tetralin formation is much faster than the rate of decalin formation. Ito et al. [37] claimed that the

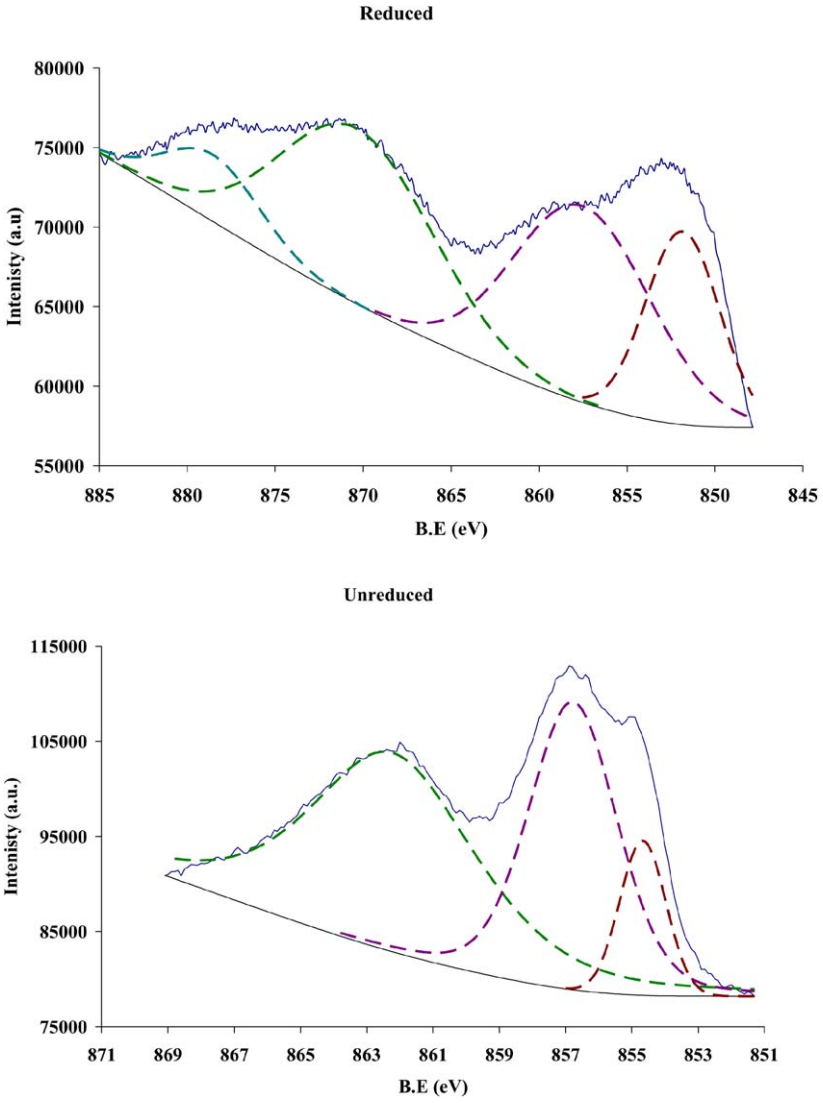


Fig. 13. XP Ni $2p_{3/2}$ spectra of reduced and unreduced NiO–$SiO_2$–$Al_2O_3$ sample; 15 wt% Ni, Si/Al = 11.

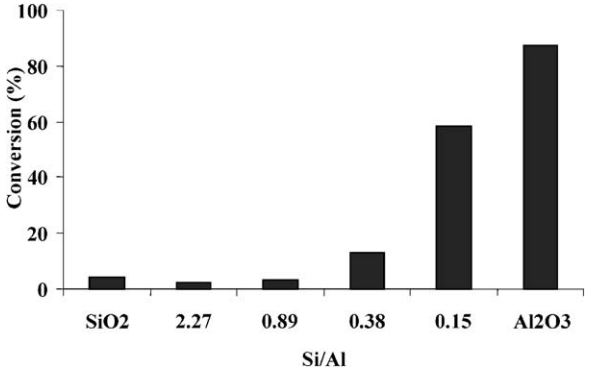


Fig. 14. Hydrogenation of naphthalene over NiO–$SiO_2$–$Al_2O_3$: effect of Si/Al ratio; WHSV = 3.3 $h^{-1}$ w.r.t. naphthalene, reaction temperature = 200 °C, reduction temperature = 300 °C, $H_2$ = 19 ml/min. Catalyst: ∼11 wt% Ni.

hydrogenation of tetralin to decalin is much faster than the hydrogenation of naphthalene to tetralin, but the low conversion of tetralin results from the greater adsorption of residual naphthalene on the active site compared with tetralin, which thus

Table 4
Product distribution in hydrogenation of toluene over NiO–$SiO_2$–$Al_2O_3$ catalysts with Si/Al ∼11 and different Ni content[a]

| Ni content (wt%) | Conversion of naphthalene (%) | Yield of tetralin (%) | Yield of decalin (%) |
|---|---|---|---|
| 0 | 0.4 | 0.4 | 0 |
| 6.8 | 20 | 20 | 0 |
| 11 | 41 | 40.8 | 0.2 |
| 15 | 47 | 46.6 | 0.4 |
| 19 | 56 | 55 | 1 |
| 40 | 75 | 71 | 4 |
| 67 | 88 | 76 | 12 |

[a] Reaction conditions: WHSV = 0.4 $h^{-1}$ w.r.t. naphthalene, reaction temperature = 200 °C, reduction temperature = 300 °C, $H_2$ = 19 ml/min.

prevents tetralin hydrogenation. Rautanen et al. [20] carried out a comprehensive kinetic study on the liquid-phase hydrogenation of naphthalene. They proposed that naphthalene adsorption occurs on a single active site, whereas tetralin adsorption requires an ensemble of Ni atoms; they used this finding to explain the different rates of hydrogenation of naphthalene and

tetralin. We have tried to obtain a reaction model to describe the hydrogenation of naphthalene based on the kinetic studies carried out over Ni–$SiO_2$–$Al_2O_3$ catalysts. To maintain isothermal conditions during the reaction, the catalyst was diluted using SiC. Van Den Bleek et al. [38] demonstrated that dilution affects the conversion during a catalytic transformation. They also proposed a criterion for determining the allowable degree of dilution without introducing errors larger than the experimental error,

$$\frac{bd_p}{l\delta} < 4 \times 10^{-3},$$

where $b$ is the fraction of inert diluent, $\delta$ is error (in percent), $l$ is the length of the undiluted catalyst bed, and $d_p$ is particle diameter. Using this criterion, we find that under our experimental conditions, dilution up to 3.3:1 was permissible within an experimental error ($\delta$) of 3%. Therefore, we used a maximum dilution of 3:1 in our kinetic studies. The absence of mass transfer limitations was evaluated using the Madon–Boudart criterion [39,40]. A ln–ln plot of activity as a function of Ni loading over $SiO_2$–$Al_2O_3$ gave a linear correlation and a slope of 1.17, which is very close to unity. This confirms that there are no mass transfer limitations under the current experimental conditions.

For any hydrogenation reaction in which the rate-limiting step is the surface reaction, the reaction rate can be described by the equation using the Langmuir–Hinshelwood model that has been widely used to describe the hydrogenation of aromatics [41]. The rate equation can be derived based on the following assumptions:

1. $H_2$ is dissociatively adsorbed over Ni surfaces, which normally is the case [42].
2. Hydrogen and the aromatic are both adsorbed on similar sites that are kinetically and thermodynamically equal [43].

For the hydrogenation of naphthalene via a two-site mechanism, the following elementary steps can be proposed:

$$H_2 + 2S \underset{k_1'}{\overset{k_1}{\longleftrightarrow}} 2H\text{–}S, \tag{1}$$

$$N + S \underset{k_2'}{\overset{k_2}{\longleftrightarrow}} N\text{–}S, \tag{2}$$

$$N\text{–}S + H\text{–}S \underset{k_3'}{\overset{k_3}{\longleftrightarrow}} NH\text{–}S + S, \tag{3}$$

$$NH\text{–}S + H\text{–}S \underset{k_4'}{\overset{k_4}{\longleftrightarrow}} NH_2\text{–}S + S, \tag{4}$$

$$NH_2\text{–}S + H\text{–}S \underset{k_5'}{\overset{k_5}{\longleftrightarrow}} NH_3\text{–}S + S, \tag{5}$$

$$H_3\text{–}S + H\text{–}S \underset{k_6'}{\overset{k_6}{\longleftrightarrow}} T\text{–}S + S, \tag{6}$$

and

$$T\text{–}S \underset{k_7'}{\overset{k_7}{\longleftrightarrow}} T + S. \tag{7}$$

Because the reaction is not operating under any diffusion limitations, the rate-limiting step is the last hydrogenation step [Eq. (6)].

The rate of the overall reaction can be written as

$$r = \frac{kP_N P_{H_2}^2 - k'P_T}{(1 + \sqrt{P_{H_2}K_{H_2}} + K_N P_N + K_T P_T)^2}. \tag{8}$$

Assuming that the reaction occurs far from equilibrium

$$r = \frac{kP_N P_{H_2}^2}{(1 + \sqrt{P_{H_2}K_{H_2}} + K_N P_N + K_T P_T)^2}. \tag{9}$$

For the hydrogenation of naphthalene via a three-site mechanism, the following steps can be proposed:

$$H_2 + 2S \underset{k_1'}{\overset{k_1}{\longleftrightarrow}} 2H\text{–}S, \tag{10}$$

$$N + S \underset{k_2'}{\overset{k_2}{\longleftrightarrow}} N\text{–}S, \tag{11}$$

$$N\text{–}S + 2H\text{–}S \underset{k_3'}{\overset{k_3}{\longleftrightarrow}} NH_2\text{–}S + 2S, \tag{12}$$

$$NH_2\text{–}S + 2H\text{–}S \underset{k_4'}{\overset{k_4}{\longleftrightarrow}} T\text{–}S + 2S, \tag{13}$$

and

$$T\text{–}S \underset{k_5'}{\overset{k_5}{\longleftrightarrow}} T + S. \tag{14}$$

The rate-limiting step as in the previous case is the last hydrogenation step [Eq. (13)].

The rate of the overall reaction can be written as

$$r = \frac{kP_N P_{H_2}^2 - k'P_T}{(1 + \sqrt{K_{H_2}P_{H_2}} + K_N P_N + K_T P_T)^3}, \tag{15}$$

and that for the reaction occurring away from the equilibrium can be written as

$$r = \frac{kP_N P_{H_2}^2}{(1 + \sqrt{K_{H_2}P_{H_2}} + K_N P_N + K_T P_T)^3}. \tag{16}$$

Both Eqs. (9) and (16) can be expressed in the general form

$$r = \frac{kP_N P_{H_2}^2}{(1 + \sqrt{K_{H_2}P_{H_2}} + K_N P_N + K_T P_T)^z}, \tag{17}$$

where $z$ is the number of active sites involved in the rate-determining step (either two or three). In a large excess of $H_2$, variations in concentration can be neglected, the $P_{H_2}$ can be considered a constant, and Eq. (17) can be rewritten as

$$r = \frac{k_1 P_N}{(K_2 + K_N P_N + K_T P_T)^z}. \tag{18}$$

Nonlinear parameter estimation of the kinetic model was performed using the Levenberg–Marquardt method. The adsorption constants of naphthalene ($K_N$) and tetralin ($K_T$) obtained from the above equation were $4.10 \times 10^{-3}$ and $1.88 \times 10^{-3}$ $m^3$/mol, respectively, at 200 °C. These values are of the same order as that reported in the literature [44]. The best fit for the equation was obtained at a $z$ value of 2. Thus the two-site

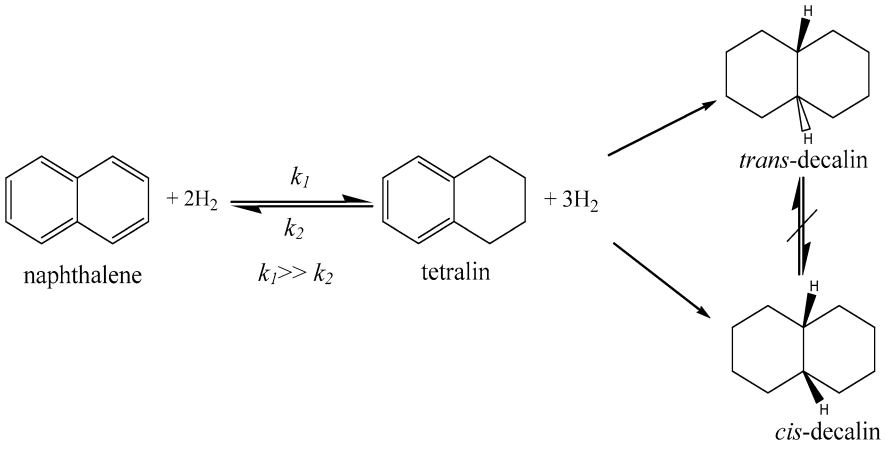


Scheme 1. Reaction pathway for the hydrogenation of naphthalene.

model best describes the hydrogenation of naphthalene over the $NiO–SiO_2–Al_2O_3$ catalysts. Based on this model, naphthalene adsorbed twice as strongly as tetralin on the catalyst surface ($K_N/K_T = 2.18$). Hence it may be concluded that hydrogenation of tetralin did not occur in the presence of naphthalene because of the competitive adsorption of naphthalene. However, when carrying out the hydrogenation of tetralin under the same reaction conditions, only 14% of it was converted to the products; 35% of the product formed was naphthalene, with the remainder decalin. This low conversion of tetralin to decalin may be the result of weak adsorption of tetralin on the surface. This hydrogenation reaction proceeds through a Langmuir–Hinshelwood model and according to this model, reaction occurs between molecules adsorbed on the surface. If one of the reactants does not adsorb or adsorbs weakly on the surface, then the reaction cannot proceed smoothly. Thus, the low conversion of tetralin to decalin in the presence of naphthalene was due not to the stronger adsorption of naphthalene, but rather to the weak adsorption of tetralin on the active sites. When decalin was passed over the catalyst under the same reaction conditions, only 1.5% of it was converted to its dehydrogenated products, tetralin and naphthalene; only about 4% of the product was naphthalene. The *cis*/*trans* ratio of the decalin was almost the same in the reactant and the product. From these studies, one can arrive at the reaction pathway in Scheme 1.

Here $k_1$ is the rate constant for naphthalene hydrogenation and $k_2$ is the rate constant for tetralin dehydrogenation. The rate of naphthalene hydrogenation was much greater than the rate of tetralin dehydrogenation, as demonstrated by the results of naphthalene hydrogenation. No significant isomerization of *trans*-decalin to *cis*-decalin (or vice versa) occurred under the current reaction conditions. Dehydrogenation of decalin to tetralin was negligible.

## 5. Conclusion

We carried out a characterization study of $NiO–SiO_2–Al_2O_3$ system prepared by a sol–gel method. The nature of the Ni species on the support was identified, and its interaction with the support was evaluated. Nickel was present in the +2 state, mostly as NiO on the catalyst. Two kinds of NiO were present, one with $Ni^{2+}$ interacting with the support and the other as free NiO (i.e., with no metal–support interactions). The concentration of free NiO species increased with increasing Ni concentration. As the amount of $SiO_2$ in the support increased, the interaction between the $Ni^{2+}$ species and the support increased. This implies that the interaction was predominantly between $Ni^{2+}$ and $SiO_2$ in the support. The reducibility of $Ni^{2+}$ therefore decreased with increasing $SiO_2$. There is a direct correlation between the hydrogenation activity of a sample and the relative concentration of the free NiO present in it before its reduction. The major product formed on hydrogenation of naphthalene was tetralin. This hydrogenation reaction was best described by a two-site Langmuir–Hinshelwood model. The adsorption constants of naphthalene ($K_N$) and tetralin ($K_T$) obtained from this model were $4.10 \times 10^{-3}$ and $1.88 \times 10^{-3}$ $m^3$/mol, respectively, at 200 °C. Naphthalene adsorbed twice as strongly as tetralin on the catalyst surface ($K_N/K_T = 2.18$). Hydrogenation of pure tetralin yielded low amounts of decalin. This proves that the low conversion of tetralin to decalin is due not to the stronger adsorption of naphthalene, but rather to the weak adsorption of tetralin on the active sites.

## Acknowledgments

This research was supported by the National Science Foundation (grant DMR-0332453). Use of the TAMU/CIMS Materials Characterization Facility and the Microscopy & Imaging Center (MIC) facility is acknowledged. The authors thank Dr. R.G. Anthony for his suggestions and comments on the kinetic studies.

## References

[1] A.T. Bell, Science 299 (2003) 1688.
[2] M.A. Cauqui, J.M. Rodriguez-Izquierdo, J. Non-Cryst. Solids 147–148 (1992) 724.
[3] S.J. Tauster, Acc. Chem. Res. 20 (1987) 389.
[4] Z. Xu, Y. Li, J. Zhang, L. Chang, R. Zhou, Z. Duan, Appl. Catal. A Gen. 210 (2001) 45.
[5] P. Turlier, H. Praliaud, P. Moral, G.A. Martin, J.A. Dalmon, Appl. Catal. 19 (1985) 287.

[6] M. Amblard, R. Burch, B.W.L. Southward, Appl. Catal. B Environ. 22 (1999) L159.
[7] S.D. Jackson, J. Willis, G.J. Kelly, G.D. McLellan, G. Webb, S. Mather, R.B. Moyes, S. Simpson, P.B. Wells, R. Whyman, Phys. Chem. Chem. Phys. 1 (1999) 2573.
[8] C. Guimon, N. El Horr, E. Romero, A. Monzon, Stud. Surf. Sci. Catal. 130D (2000) 3345.
[9] M.A. Keane, P.M. Patterson, Ind. Eng. Chem. Res. 38 (1999) 1295.
[10] P.D. Tien, T. Satoh, M. Miura, M. Nomura, Energy Fuels 19 (2005) 731.
[11] L. Sun, Z. Zong, J. Kou, L. Zhang, Z. Ni, G. Yu, H. Chen, X. Wei, Energy Fuels 18 (2004) 1500.
[12] T. Enya, H. Suzuki, T. Watanabe, T. Hirayama, Y. Hisamatsu, Environ. Sci. Technol. 31 (1997) 2772.
[13] V.D. Berg, J.P. Lucien, G. Germaine, G.L.B. Thielemans, Fuel Process. Technol. 35 (1993) 119.
[14] A. Corma, A. Martinez, V.M. Soria, J. Catal. 200 (2001) 259.
[15] A. Stanislaus, B.H. Cooper, Catal. Rev. Sci. Eng. 36 (1994) 75.
[16] J.A. Pena, J. Herguido, C. Guimon, A. Monzon, J. Santamaria, J. Catal. 159 (1996) 313.
[17] V.L. Barrio, P.L. Arias, J.F. Cambra, M.B. Güemez, B. Pawelec, J.L.G. Fierro, Appl. Catal. A Gen. 242 (2003) 17.
[18] M. Mandreoli, A. Vaccari, E. Veggetti, M. Jacquin, D.J. Jones, J. Roziere, Appl. Catal. A Gen. 231 (2002) 263.
[19] R.G. Reynoso, J. Ramırez, R. Nares, R. Luna, F. Murrieta, Catal. Today 107–108 (2005) 926.
[20] P.A. Rautanen, M.S. Lylykangas, J.R. Aittamaa, A.O.I. Krause, Ind. Eng. Chem. Res. 41 (2002) 5966.
[21] P.A. Rautanen, M.S. Lylykangas, J.R. Aittamaa, A.O.I. Krause, Stud. Surf. Sci. Catal. 133 (2001) 309.
[22] B.G. Shpeizer, A. Clearfield, J.M. Heising, Chem. Commun. 18 (2005) 2396.
[23] A.M. Venezia, V. La Parola, B. Pawelec, J.L.G. Fierro, Appl. Catal. A Gen. 264 (2004) 43.
[24] G. Poncelet, M.A. Centeno, R. Molina, Appl. Catal. A Gen. 288 (2005) 232.
[25] B. Mile, D. Stirling, M.A. Zammitt, A. Lovell, M. Webb, J. Mol. Catal. 62 (1990) 179.
[26] T. Tsonchevaa, M. Linden, J. Rosenholm, C. Minchev, React. Kinet. Catal. Lett. 86 (2005) 275.
[27] S. Xu, X. Wang, Fuel 84 (2005) 563.
[28] J.M. Rynkowski, T. Paryjczak, M. Lenik, Appl. Catal. A Gen. 106 (1993) 73.
[29] F. Arena, R. Dario, A. Parmaliana, Appl. Catal. A Gen. 170 (1998) 127.
[30] F. Medina, P. Salagre, J.E. Sueiras, J. Chem. Soc. Faraday Trans. 89 (1993) 3507.
[31] S.D. Lin, C. Song, Catal. Today 31 (1996) 93.
[32] T. Kotanigawa, M. Yamamoto, T. Yoshida, Appl. Catal. A Gen. 164 (1997) 323.
[33] A.Yu. Stakheev, L.M. Kustov, Appl. Catal. A Gen. 188 (1999) 3.
[34] G. Pina, C. Louis, M.A. Keane, Phys. Chem. Chem. Phys. 5 (2003) 1924.
[35] C. Park, M.A. Keane, J. Colloid Interface Sci. 266 (2003) 183.
[36] A. Corma, A. Martinez, V. Martines-Soria, J. Catal. 169 (1997) 480.
[37] K. Ito, Y. Kogasaka, H. Kurokawa, M. Ohshima, K. Sugiyama, H. Miura, Fuel Process. Technol. 79 (2002) 77.
[38] C.M. Van Den Bleek, K. Van Der Wiele, P.J. Vanden Berg, Chem. Eng. Sci. 24 (1969) 681.
[39] R.J. Madon, M. Boudart, Ind. Eng. Chem. Fundam. 21 (1982) 438.
[40] U.K. Singh, M.A. Vannice, J. Catal. 199 (2001) 73.
[41] R.C. Santana, S. Jongpatiwut, W.E. Alvarez, D.E. Resasco, Ind. Eng. Chem. Res. 44 (2005) 7928.
[42] K. Nobuhara, H. Kasai, W.A. Dino, H. Nakanishi, Surf. Sci. 566–568 (2004) 703.
[43] C.D. Holland, R.G. Anthony, Fundamentals of Chemical Reaction Engineering, Prentice–Hall, Englewood Cliffs, NJ, 1979.
[44] M.S. Lylykangas, P.A. Rautanen, A.O.I. Krause, Ind. Eng. Chem. Res. 41 (2002) 5632.